Mitigating the Effect of High Overpotential during Al Deposition on Aluminium-Graphite Battery Performance

Charan Mukundan[a] and Jean-Francois Drillet*[a]

This study investigates the impact of current density on electrode potential during aluminium (Al) dissolution/deposition step from/on an Al foil as well as the charge-discharge behaviour of aluminium-graphite batteries (AGB) in various $AlCl_3$-based electrolytes. Preliminary experiments in a cell with graphite blocking electrodes evidenced higher chemical stability of 1:1.5 Urea:$AlCl_3$ electrolyte, followed by 1:1.5 TEA:$AlCl_3$ and 1:1.5 EMIMCl:$AlCl_3$. In Al—Al symmetric cells, current densities above 1 mA cm^{-2} led to a notable rise in overpotential up to 100 mV during Al deposition in both TEA:$AlCl_3$ and Urea:$AlCl_3$ electrolytes mostly due to low surface area of native Al foil. Similar trend was observed in AGB full cells, where higher overpotentials during Al deposition caused 'incomplete' $AlCl_4^-$ intercalation in natural graphite (NG), resulting in capacity fade at current densities in the range between 0.5 and 5 A g^{-1}. By adjusting the upper cut-off voltage (UCV) during charging step as a function of applied current value according to respective electrolyte stability, a significant improvement in specific capacity and energy density was achieved during charging and discharging steps. For instance at 1 A g^{-1}, the specific energy density of AGB increased by 10% in EMIM-Cl:$AlCl_3$, 48% in TEA:$AlCl_3$, and an impressive 250% in Urea:$AlCl_3$.During long-term cycling post-UCV adjustment, the capacities of AGB increased by 10%, 13%, and 27% for AGBs with EMIMCl:$AlCl_3$, TEA:$AlCl_3$ and Urea:$AlCl_3$, respectively with a negligible capacity fade of less than 1% for EMIMCl:$AlCl_3$ and TEA:$AlCl_3$, and a 9% capacity fade for Urea:$AlCl_3$.

1. Introduction

The global focus on reducing reliance on fossil fuels has led to an increased demand for renewable energy sources like solar, wind, and hydropower. However, a major challenge is related to the huge logistic required for large-scale energy storage and distribution.[1,2] Rechargeable batteries meeting criteria such as high capacity, affordability, stability, and durability emerge as one of viable solutions for storing energy from fluctuating and unpredictable, renewable sources.[3] Over the past few decades, the lithium-ion battery (LIB) market has grown significantly to address the rising need for energy storage in various applications, including consumer electronics, on-grid systems, and transportation.[4] Yet, challenges such as limited resources and escalating costs of lithium and cobalt have prompted exploration into battery technologies based on more abundant metals like sodium, aluminium, zinc, magnesium, potassium, and calcium.[5] Among these, aluminium stands out due to its high theoretical gravimetric energy (2.98 Ah g^{-1}), nearly 80% of that of lithium (3.86 Ah g^{-1}) due to its higher gram-equivalent weight (GEW) (8.97 vs. 6.94 g/eq for Li). The GEW is calculated from ratio of molecular/atomic weight divided by the number of electrons involved in the reaction assuming that 1 gram of equivalent weight of active material can theoretically deliver 26.8 Ah.[6] The lower the GEW value the higher the specific capacity. Due to the higher density of Al material (2.69 vs. 0.54 g cm^{-3} for Li), theoretical value of volumetric capacity of Al amounts to 8.04 vs. 2.06 Ah cm^{-3} for metallic Li. Moreover, Aluminium-graphite batteries (AGBs) rely on low-cost, abundant, non-flammable, and easily recyclable materials such as aluminium for the positive electrode and graphite for the negative electrode. It should be noted that the capacity of AGBs is primarily limited by the graphite material, if there is an excess of electrolyte, particularly with sufficient concentrations of $Al_2Cl_7^-$ ions.[7,8] However, AGB technology faces some challenging issues related to Al dendrite growth,[9] Al passivation,[10,11] and cost of EMIMCl:$AlCl_3$ chloroaluminate electrolyte[12] as well as relatively low gravimetric and volumetric capacity at cell level.[13]

A promising way to mitigate Al dendrite growth is to optimise the surface of the Aluminium electrode.[9,14,15] Due to their exceptional chemical stability and high porosity (>80%), thick glass fiber (GF) separators, ranging from 260 to 650 μm in thickness, are commonly used in most published studies. However, this design promotes aluminium growth from the Al anode toward the cathode, leading to short circuits and their thickness strongly affects the volumetric cell density.[16] Therefore, replacing the traditional GF separator with a less porous separator/membrane that functions as both dendrite barrier and electrolyte reservoir is crucial for improving AGB technology.[12] In our recent work, we demonstrated for the first time that a polyether sulfone membrane (PES) of 160 μm in thickness can be a very promising separator for AGBs.[17] To

[a] C. Mukundan, Dr. J.-F. Drillet
     Energy storage and conversion team,
     DECHEMA Forschungsinstitut, Theodor-Heuss-Allee 25, 60486 Frankfurt am Main
     E-mail: jean-francois.drillet@dechema.de

Batteries & Supercaps

Research Article
doi.org/10.1002/batt.202400718

Chemistry Europe
European Chemical
Societies Publishing

prevent the passivation of the Al electrode, highly pure aprotic electrolytes such as $EMIMCl:AlCl_3$ chloroaluminate are required.[18] While the $EMIMCl:AlCl_3$ ionic liquid mixture performs very well, there is considerable interest in exploring the feasibility of less corrosive and cheaper $AlCl_3$-based mixtures such as triethylamine hydrochloride (TEA),[19,20] trimethylamine hydrochloride (TMA),[21] urea,[22,23] caprolactam,[24] and acetamide.[25,26]

The specific capacity of AGBs is largely determined by the nature and loading of the graphitic material, which must accommodate the considerably large $AlCl_4^-$ anions (5.8 Å),[27] in contrast to the much smaller Li^+ ions (0.59 Å),[2] as well as the constraints imposed by the electrolyte stability window (ESW).[18] According to density functional theory (DFT) calculations, a 6x6 graphene sheet composed of 72 carbon atoms can host up to four $AlCl_4^-$ intercalants, which corresponds to 18 carbon atoms per $AlCl_4^-$.[28] This arrangement allows for a maximum theoretical capacity of 124 mAh g^{-1} when achieving full intercalation even up to *stage-1*, where each graphene layer is intercalated with $AlCl_4^-$ ions to form graphite intercalated compounds (GIC). For comparison, Li^+ intercalation up to *stage-1* can yield a maximum theoretical capacity of 372 mAh g^{-1} by forming LiC_6 GICs.[29] Due to the limited stability window of the $EMIMCl:AlCl_3$ electrolyte of 2.45 V vs Al/Al^{3+}, the graphite cathode typically only reaches up to *stage-4* intercalation.[30] Moreover first-principles calculations show that the large size of the $AlCl_4^-$ anion ($\sim$5.28 Å)[31] might significantly increase the graphene layer interlayer distance up to 8.8 Å.[28,32] Surprisingly, experimental analysis indicates an increase in gallery height up to "only" 5.7 Å for $AlCl_4$-GIC, representing a 160% expansion compared to the pristine graphite gallery height of 3.5 Å.[27]

More generally, graphite with higher crystallinity, as evidenced by its nearly perfect interplanar d-spacing of 0.3354 nm at room temperature and the low intensity of the D-band in Raman spectra, demonstrates superior charge-discharge performance in AGBs.[33] Wang et al. showed that a cell with large flakes of natural graphite with I_d/I_g ratio of 0.09 and interplanar d-spacing of 0.3356 showed a capacity of 100 mAh g^{-1} compared to only 75 mAh g^{-1} for small graphite flakes with I_d/I_g ratio of 0.27 and interplanar d-spacing of 0.3371 nm.[34] Further graphitic materials including graphene,[35–38] kish graphite,[34] and expanded graphite[39–41] have been evaluated, whereas cost-effective, commercially available expanded graphite synthesised by chemical oxidation or high temperature exfoliation methods appears to be more suitable for industrial scaling of AGBs.[41,42]

Another significant issue in AGB is the higher overpotential observed at the Al foil anode during aluminium electrodeposition step (charging) of AGBs at high current densities ($>$1 A g^{-1}). Various approaches for optimizing anode morphology have been successfully implemented, such as chemical treatment of the aluminium foil surface,[9,43] coating with aluminium powder,[44] removal of oxide layers through electropolishing,[45,46] or using graphite layer as a substrate for aluminium deposition.[16,47] In addition to the optimisation of Aluminium anode surface, electrolyte nature plays a major role. In a previous work, we reported on AGBs using a TEA-AlCl$_3$ electro-

lyte, where the capacity increased from 60 to 90 mAh g^{-1} during long-term cycling at 1 A g^{-1}.[19] This improvement was primarily due to a continuous reduction in the aluminium anode overpotential with increasing cycles, enabling 'complete' charging of the graphite cathode up to 2.37 V vs Al/Al^{3+}, and consequently, an increase in capacity over time. This study aims to explore the influence of both current density ranging from 0.1 to 5 A g^{-1} and electrolyte nature ($EMIMCl:AlCl_3$, $TEA:AlCl_3$, and $Urea:AlCl_3$) on anode and cathode overpotential behaviour. By adjusting the upper cut-off voltage (UCV) during the charging step, an impressive increase in AGB cell performance in terms of specific capacity especially in $TEA:AlCl_3$ electrolyte was achieved.

2. Results and Discussion

2.1. Physical Characterisation of Pristine Natural Graphite Powder

The FESEM images in Figure 1a reveals that the natural graphite (NG) used in this study has a potato shaped morphology with an average particle size of 17 μm. The Raman spectra of the NG sample in Figure 1b shows characteristic peaks of D, G and 2D bands at around 1360, 1575, and 2710 cm^{-1}, respectively with an I_D/I_G ratio of 0.106 indicating a high graphitization degree of the material.
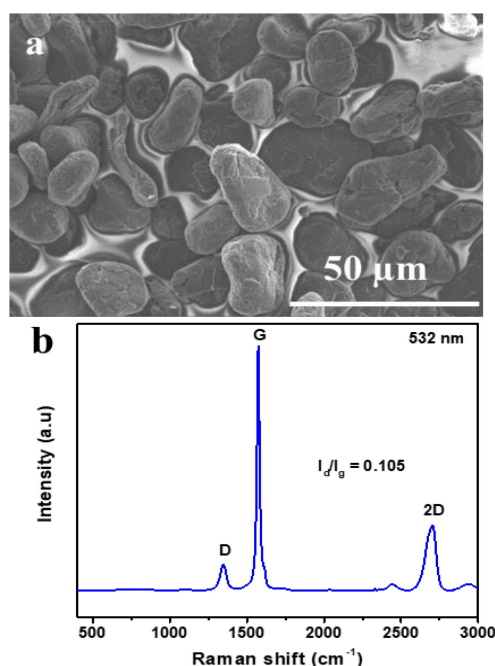

Figure 1. (a) SEM image, and (b) Raman spectra of the natural graphite.
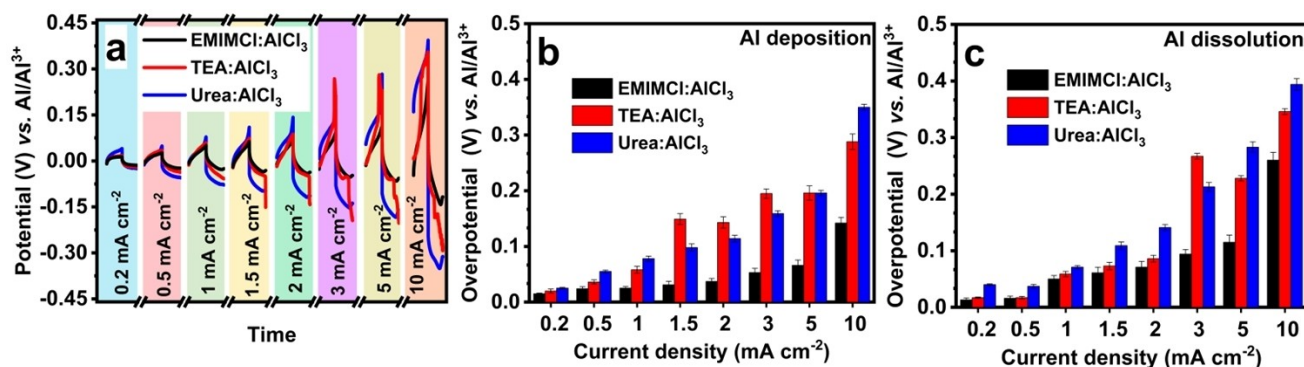
Figure 2. (a) Voltage vs time curve of 10th cycle of Al dissolution-deposition process, and average overpotential value at the end of (b) deposition and (c) dissolution step at different current densities in Al–Al symmetric cell.

2.2. Influence of the Electrolyte Composition on the Al Deposition-Dissolution Process

The influence of electrolyte nature ($EMIMCl:AlCl_3$, $TEA:AlCl_3$ and $Urea:AlCl_3$) on aluminium deposition and dissolution reactions was investigated in an Al–Al symmetric cell at current densities ranging from 0.2 to 10 mA cm^{-2} as tabulated in table S1, with a fixed absolute capacity of 0.159 mAh (equivalent to 0.2 mAh cm^{-2}). Figure 2a–c presents the whole voltage curve profiles during anodic (Al dissolution) and cathodic (Al deposition) scan at the 10th cycle step and the mean overpotential values of the vertex potential as bar diagram for the 10 cycles in the Al–Al symmetrical cell. Figure 2a, clearly shows that the best performance in terms of overpotential for both Al deposition and stripping was consistently achieved with $EMIMCl:AlCl_3$, followed by $TEA:AlCl_3$ and $Urea:AlCl_3$. Within Al deposition range of 1–3 mA cm^{-2}, however, overpotential values were about 30–50 mV higher in $TEA:AlCl_3$ than in $Urea:AlCl_3$. In summary as shown in Figure 2b&c, the overpotential values for both Al reactions increased on average from 25–30 mV at 0.2 mA cm^{-2} up to 140–360 mV at 10 mA cm^{-2}. The overpotential of Al deposition reaction in $TEA:AlCl_3$ sharply increased up to 148, 195 and 288 mV at 1.5, 3 and 10 mA cm^{-2}, respectively. This rise can be attributed to the higher viscosity and lower ionic conductivity of the $TEA:AlCl_3$ electrolyte ($\eta = 22.3$ mPa s and $\sigma = 9.50$ mS cm^{-1} at 20 °C).[48] compared to $EMIMCl:AlCl_3$ ($\eta = 15.7$ mPa s and $\sigma = 16.35$ mS cm^{-1} at 25 °C).[48,49] In Urea:AlCl$_3$, the overpotential during aluminium deposition ranged from 25 to 98 mV at current densities of 0.2 to 1.5 mA cm^{-2}. However, at higher current densities between 2 and 10 mA cm^{-2}, the overpotential jumped from 141 up to 394 mV. The overpotential during aluminium dissolution followed a similar trend, as illustrated in Figure 2c. The significant variation in overpotential during Al dissolution/deposition process, particularly at elevated current densities, can be attributed to mass transport limitation due to high viscosity and low ionic conductivity of 1:1.5 Urea:AlCl$_3$ ($\eta = 218$ mPa.s and $\sigma = 1.6$ mS cm^{-1} at 20 °C).[50]

2.3. Influence of Electrolyte Nature and Electrochemical Stability on AlCl$_4^-$ Intercalation/Deintercalation Behaviour in NG

The cyclic voltammograms (CV) of NG at a scan rate of 1 mV s^{-1} (Figure 3a) showed significant differences in the anodic and cathodic peaks between ionic liquids (ILs) $EMIMCl:AlCl_3$ and $TEA:AlCl_3$ and deep eutectic solvent (DES) $Urea:AlCl_3$. In $EMIMCl:AlCl_3$ and $TEA:AlCl_3$, three major oxidation peaks during positive scan suggest multiple stages or pathways for AlCl$_4^-$ anion intercalation into graphite matrix.[30] Comparing the CV to
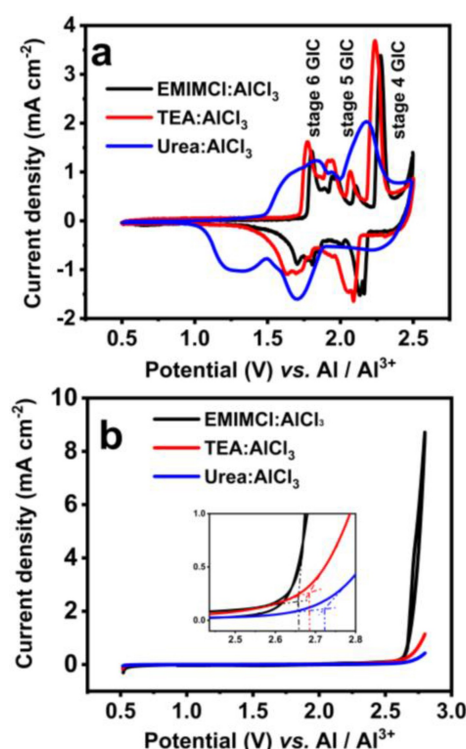

Figure 3. a) CVs obtained in a three-electrode configuration using natural graphite as working electrode in different electrolytes within a potential window of 0.5–2.5 V at a scan rate of 1 mV s^{-1}, b) Electrolyte stability window with glassy carbon rod as working and counter blocking electrode within a potential window of 0.5–2.8 V at a scan rate of 1 mV s^{-1}.

Batteries & Supercaps

Research Article
doi.org/10.1002/batt.202400718

**Chemistry
Europe**

European Chemical
Societies Publishing

the results reported by Pan et al.,[30] the oxidation peak between 1.7 to 2.0 V is associated to the intercalation of $AlCl_4^-$ anions every sixth graphene layer, noted as *stage-6* intercalation. The subsequent peak from 2.0 to 2.1 V indicated *stage-5* intercalation, while distinct and predominant peak at 2.2 V (2.1–2.37 V) corresponds to *stage-4* intercalation process.[30,51] Corresponding reduction peaks between 1.25–1.7 V and 2.25–1.75 V underscore the reversibility of $AlCl_4^-$ intercalation processes. Although the redox peaks in EMIMCl:AlCl$_3$ and TEA:AlCl$_3$ are similar, the slight difference in offset potential (30 mV) of $AlCl_4^-$ intercalation in TEA:AlCl$_3$ may be indicative of more favourable kinetics compare to that in EMIMCl:AlCl$_3$. Conversely, in the Urea:AlCl$_3$ mixture, oxidation peaks shifted to lower potentials compared to those observed in ILs (EMIMCl:AlCl$_3$ and TEA:AlCl$_3$). The shift may be attributed to the differences in kinetics that arise from interactions between $AlCl_4^-$ and the $[AlCl_2(ligand)_2]^+$ species in Urea:AlCl$_3$ and is different from $AlCl_4^-/Al_2Cl_7^-$ interactions in ILs.[25,50,52]

The presence of two oxidation peaks in the 1.4–2 V range and another between 2–2.27 V, alongside two reversible peaks in 1.85–1.5 V and 1.5–1.0 V, suggests distinct electrochemical reactions associated with $AlCl_4^-$ anion intercalation-deintercalation process in NG structure in Urea:AlCl$_3$. Similarly, the broader peaks observed during $AlCl_4^-$ anion intercalation-deintercalation process in NG with Urea:AlCl$_3$ is likely due to $\approx$ 10 times higher viscosity and lower conductivity that obviously affect mass transport and consequently kinetics of $AlCl_4^-$ anion processes.[25] The stability window of 1:1.5 EMIMCl:AlCl$_3$, TEA:AlCl$_3$, and Urea:AlCl$_3$ electrolytes shown in Figure 3b was evaluated up to 2.8 V. At 0.5 mA cm^{-2}, lowest onset potential of electrolyte decomposition occurred at 2.65 V and 2.72 V for EMIMCl:AlCl$_3$ and TEA:AlCl$_3$, respectively compared to 2.8 V for more chemically stable Urea:AlCl$_3$ mixture.

2.4. AGB Full-Cell Experiments

The optimal upper cut-off voltage (UCV) for the AGB cell in different electrolytes was determined at a current density of 0.1 A g^{-1}, aiming to achieve a similar coulombic efficiency (CE) of 98.5%, as illustrated in Figure S1. The UCV was set as 2.40 V for cells using EMIMCl:AlCl$_3$ and Urea:AlCl$_3$ while a slightly higher UCV of 2.45 V was set for cells employing TEA:AlCl$_3$. As shown in Figure S1, at a cut-off voltage of 2.45 V, the cells with EMIMCl:AlCl$_3$ and Urea:AlCl$_3$ exhibited a CE of 87.5% and 91%, respectively. Figure 4a illustrates the charge-discharge behaviour of the AGB cell during the 25th cycle at a current density of 0.1 A g^{-1}. The highest specific capacity and energy during discharge step was achieved in the cell with TEA:AlCl$_3$ (~95 mAh g^{-1}; 171 mWh g^{-1}) followed by EMIMCl:AlCl$_3$ (~90 mAh g^{-1}; 164 mWh g^{-1}) and Urea:AlCl$_3$ (~84 mAh g^{-1}; 140 mWh g^{-1}).

The superior performance and CE of cell with TEA:AlCl$_3$ compared to EMIMCl:AlCl$_3$ and Urea:AlCl$_3$ is also attributed to the higher cut-off voltage (by 50 mV) during charging step. The reason for enhanced ESW for TEA:AlCl$_3$ can be explained by the cation-anion interaction energy (ΔE_{int}) determined by density functional theory (DFT) calculations reported by Azimi et al.[48] These calculations reveal that TEA:AlCl$_3$ forms stronger coulombic and hydrogen bonding interactions than EMIMCl:AlCl$_3$ facilitated by the formation of six hydrogen bonds between TEAH$^+$ and chloroaluminate anions in contrast to only three hydrogen bonds for EMIM$^+$. While the charge/discharge profiles of AGB with EMIMCl:AlCl$_3$ and TEA:AlCl$_3$ exhibit similar characteristics and plateaus, the profile of AGB with Urea:AlCl$_3$ is different signified by a lower cell voltage during both charging (220–230 mV) and discharging (250–280 mV) step. Nevertheless, the specific capacity of AGB with Urea:AlCl$_3$ amounts to 83 mAh g^{-1} which is comparable to its performance with other ILs, whereas cell discharge voltage is also lowing strongly affecting the specific cell energy density with respect to the mass of graphite (Figure 8b). During the charging step (Figure 4b), the overpotential of the Al anode at EoC, corresponding to the aluminium electrodeposition process, notably varied among the electrolytes, emphasizing the strong influence of the electrolyte nature. The overpotential values of Al anode at EoC in EMIMCl:AlCl$_3$, TEA:AlCl$_3$, and Urea:AlCl$_3$ were 0.06 V, 0.033 V, and 0.07 V, vs. Al/Al^{3+} respectively. Correspondingly (Figure 4c), the electrode potential of NG at EoC was measured as 2.34, 2.42 V, and 2.33 V vs. Al/Al^{3+} in EMIMCl:AlCl$_3$, TEA:AlCl$_3$, and Urea:AlCl$_3$, respectively.
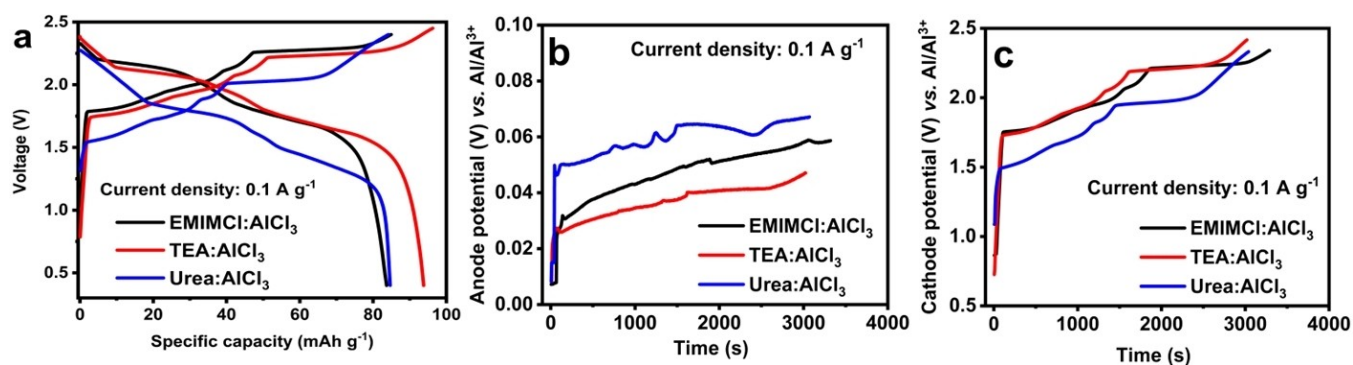

Figure 4. Comparison of a) 25th charge-discharge curves of AGB during galvanostatic cycling in different electrolytes at 0.1 A g^{-1} with respective b) anode and c) cathode potential curves during charging step.

Batteries & Supercaps

Research Article
doi.org/10.1002/batt.202400718

Chemistry Europe
European Chemical
Societies Publishing

2.5. Rate Capability

Figure 5 shows the rate capability of the AGB from a current density of 0.1 to 5 A g^{-1}. Notably, the AGB utilizing TEA:AlCl$_3$ demonstrates superior capacity retention, particularly at lower current densities. At 0.25 A g^{-1}, the specific capacities of the cells with EMIMCl:AlCl$_3$, TEA:AlCl$_3$, and Urea:AlCl$_3$ are 88.3, 94.4, and 84.9 mAh g^{-1}, corresponding to the capacity retention of 98, 97, and 94% respectively, compared to their initial values at 0.1 A g^{-1} (88.7, 94.3, and 84.9 mAh g^{-1}). However, a decline in capacity is observed at 0.75 A g^{-1}, dropping to 81.3, 89.7, and 63.8 mAh g^{-1} (72, 90, and 75% capacity retention) for the respective electrolytes. This trend further intensifies at 1 A g^{-1},

where capacity decreases to 64.8, 79.9, and 39.6 mAh g^{-1}. At higher current densities, cells with EMIMCl:AlCl$_3$ and TEA:AlCl$_3$ exhibit retention of 55 and 52% (at 2 A g^{-1}) and 39 and 32% (at 5 A g^{-1}), respectively. Conversely, cells using Urea:AlCl$_3$ show almost a complete capacity depletion at these high current densities.

Figure 6 illustrates the impact of electrolyte composition and current density on the charge-discharge behaviour (Figure 6a,c,e), as well as the potentials of the Al anode and NG cathode (Figure 6b,d,f) during the charging process. As expected, both electrolyte composition as well as current density exert a substantial influence on the potentials of the NG cathode and Al anode during the charging process (SI Table S2). These factors subsequently influence the overall capacity of AGBs, as demonstrated in Figure 6. With EMIMCl:AlCl$_3$, a consistent and gradual increase in anode potential is observed as the current density rises from 0.1 A g^{-1} to 5 A g^{-1}, alongside a steady decrease in cathode potential from 2.333 V to 2.049 V (Figure 6a). The consistent potential changes on anode and cathode are reflected in the gradual decrease in capacity (especially from last charging plateau) from the charge-discharge curves (Figure 6b). In contrast, AGB with TEA:AlCl$_3$ (Figure 6c) shows a similar trend in cathode potential reduction which reduces from 2.42 V to 2.02 V, but the anode potential exhibits a more rapid increase, moving from 0.033 V to 0.359 V. This suggests that cell with TEA:AlCl$_3$ is less efficient at higher current densities which is evident by looking at abrupt transitions observed in the charge-discharge curves (Figure 6d). Cell using Urea:AlCl$_3$ electrolyte displays the most dramatic change as Al anode overpotential potentials increased significantly (Figure 6e), leading to AGB delivering almost no capacity at 5 A g^{-1} (Figure 6f). These variations are attributed to the diffusion limitations of AlCl$_4^-$ intercalation/deintercalation with-
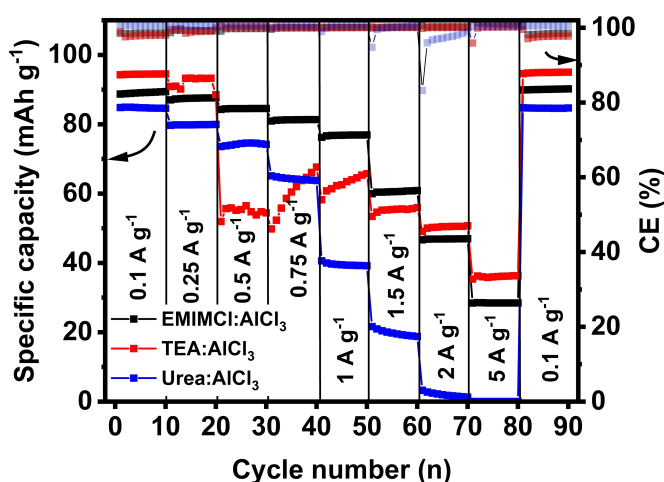

Figure 5. Comparison of specific capacity and coulombic efficiency (CE) of AGB in different electrolytes cycled at different current densities. The experiments were carried out after 25 activation cycles at 0.1 A g^{-1} shown in Figure 4a.
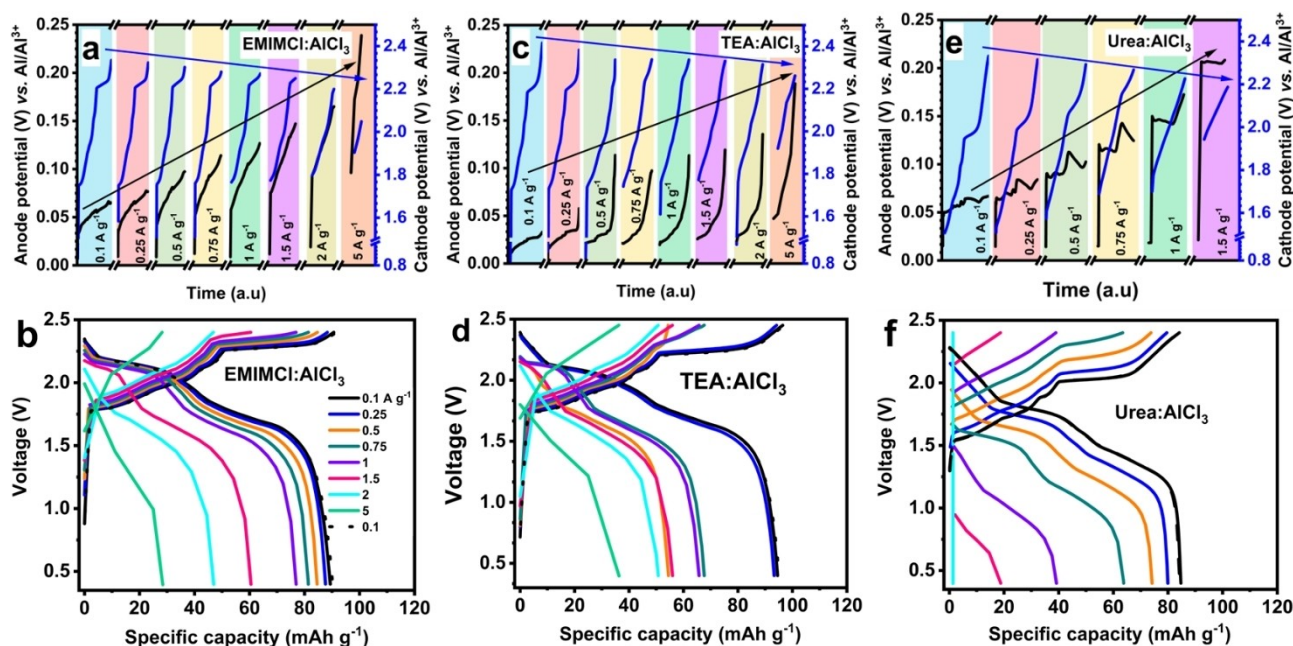

Figure 6. Comparison of potential of Al anode and natural graphite cathode during charging step at different current densities in a) EMIMCl:AlCl$_3$ c) TEA:AlCl$_3$ and e) Urea:AlCl$_3$. Comparison of charge-discharge curves at different current densities in b) EMIMCl:AlCl$_3$, d) TEA:AlCl$_3$ and f) Urea:AlCl$_3$.

Batteries & Supercaps

Research Article
doi.org/10.1002/batt.202400718

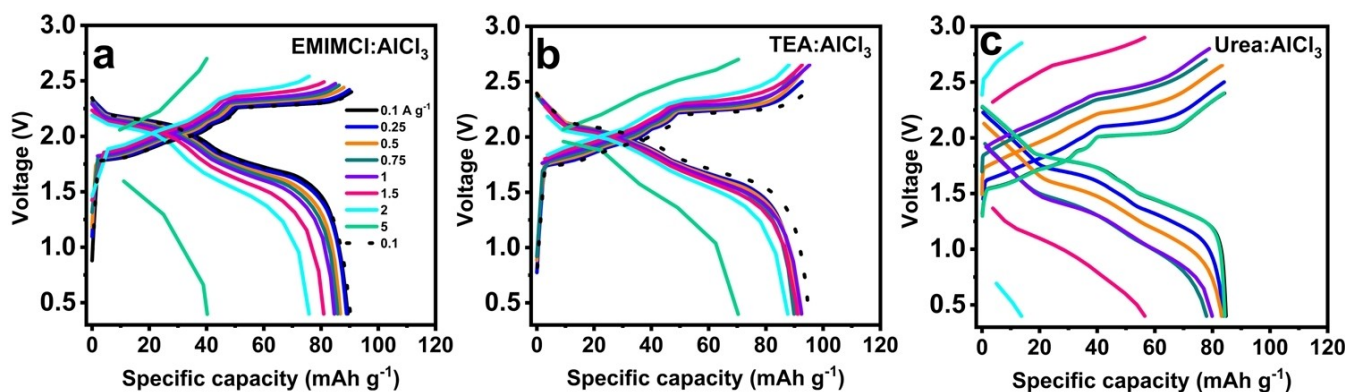**Chemistry Europe**
European Chemical
Societies Publishing

Figure 7. Comparison of charge-discharge curves at different current densities after adjusted UCV during charging step in a) EMIMCl:AlCl$_3$, b) TEA:AlCl$_3$ and c) Urea:AlCl$_3$.

in the graphite layers at higher current densities,[53] as well as factors like ion-pair interactions, viscosity, and ion complex formation affecting ion mobility and conductivity of each electrolyte whose influence were also observed in Al–Al symmetric cells.[48] The observed increase in the anode potential at EoC during the charging process with increase in current density in the AGB cell closely resembles the pattern of the Al electrode potential during the Al deposition process in the Al–Al symmetric cell (Figure 2a). Particularly noteworthy is the drastic surge in the Al electrode potential during Al deposition in TEA:AlCl$_3$ in both the AGB full cell and the Al–Al symmetric cell from the current densities of 0.5 Ag^{-1} and 1.5 mA cm^{-2}, respectively that confirms the poor efficiency of the Al deposition process in that electrolyte at higher current densities.

In contrast, the maximum achievable specific capacity of AGB in EMIMCl:AlCl$_3$, TEA:AlCl$_3$, and Urea:AlCl$_3$ is realized only when the NG cathode approaches the potentials of 2.34 V, 2.417 V, and 2.332 V potential at EoC, respectively (Figure 4c), which is a determining factor for the overall capacity.[54] Hence, a lower potential of NG cathode at EoC at higher current densities can be an indication of an 'incomplete' or partial charging process of NG, elucidating another possible reason for the observed capacity fade with an increase in current density. To mitigate the effects of increased overpotentials on the Al anode during charging process, the UCV of the AGB cell was meticulously adjusted for each current density (see Table S3).

Importantly, higher cut-off voltages did not affect the Mo current collector, which demonstrates electrochemical stability up to 2.5 V versus Al/Al^{3+}.[19] Moreover, the cathode potential consistently stayed below this threshold until the EoC, ensuring safe operation within the electrochemical stability limits of the materials involved. The impact of cut-off voltage adjustment on the specific capacity and the capacity retention (vs. at 0.1 Ag^{-1}) especially at higher current densities from 0.5 to 5 Ag^{-1} is clearly observed in the AGB cell across all electrolytes, as shown in Figure 7 (a–c) and Figure S3. Figure 8a shows that at 0.5 Ag^{-1}, the specific capacity of AGB with TEA:AlCl$_3$ increased substantially by ~36 mAh g^{-1} compared to the average specific capacity before UCV adjustment at the same current density,
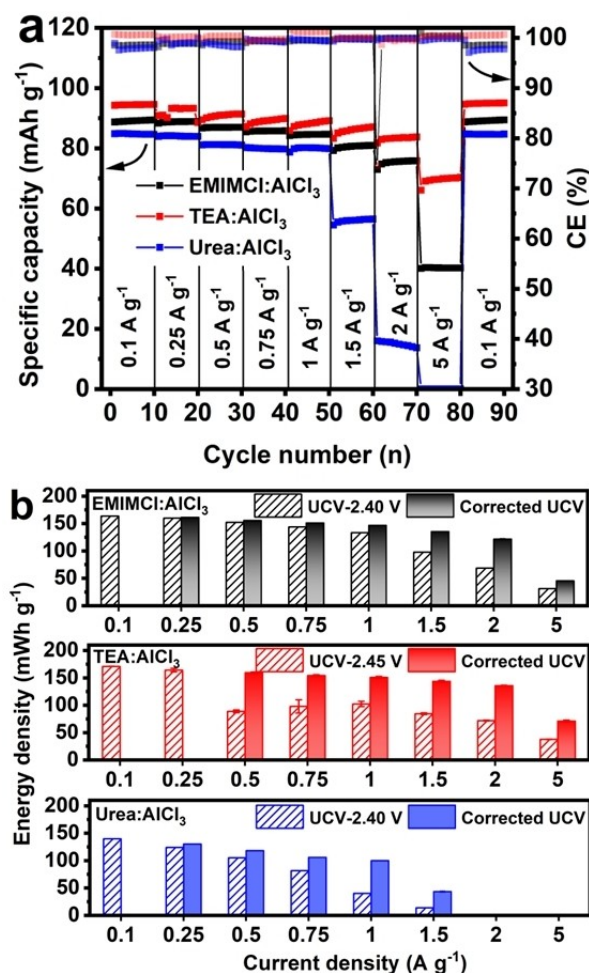

Figure 8. Comparison of a) specific capacity and coulombic efficiency (CE) of Al-NG AIB in different electrolytes cycled at different current density after UCV adjustment and b) energy density of NG cathode at different current densities between before and after UCV adjustment.

while the cell with EMIMCl:AlCl$_3$ and Urea:AlCl$_3$ showed smaller gains of ~2.5 mAh g^{-1} and ~7 mAh g^{-1}, respectively. At 1 Ag^{-1}, the capacity of AGB with EMIMCl:AlCl$_3$ increased by ~8 mAh g^{-1}, with TEA:AlCl$_3$ and Urea:AlCl$_3$ improved by ~25 mAh g^{-1} and ~40 mAh g^{-1}, respectively. At 2 Ag^{-1}, AGB

Batteries & Supercaps

Research Article
doi.org/10.1002/batt.202400718

Chemistry
Europe
European Chemical
Societies Publishing

with TEA:AlCl$_3$ showed a significant increase by 33 mAh g^{-1}. Following the adjustment of UCV for different current densities, the cathode potential at EoC in EMIMCl:AlCl$_3$, TEA:AlCl$_3$, and Urea:AlCl$_3$ remained consistent at 2.34 V, 2.417 V, and 2.332 V, respectively, across all current densities (Figure S2) indicating 'complete' charging of NG. Owing to substantial enhancements in AGB capacities across all electrolytes up to 2 A g^{-1} following UCV adjustments, an increase in the energy density of the NG cathode (reported energy densities were normalized to the mass of graphite) is evident, particularly at higher current densities, as depicted in Figure 8b. Notably, at 1 A g^{-1}, the energy density of NG increased by 10% in EMIMCl:AlCl$_3$, 48% in TEA:AlCl$_3$, and an impressive 250% in Urea:AlCl$_3$ after the UCV adjustment. Despite encountering capacity fade at 2 A g^{-1} in Urea:AlCl$_3$, the energy density of NG witnessed a remarkable 300% increase in Urea:AlCl$_3$, 70% in TEA:AlCl$_3$, and 40% in EMIMCl:AlCl$_3$.

2.6. Long-Term Cycling

The long-term stability of AGBs was investigated in different electrolytes over a testing period of 1000 cycles at 1 A g^{-1} and the results are shown in Figure 9a. Initially, the cell with
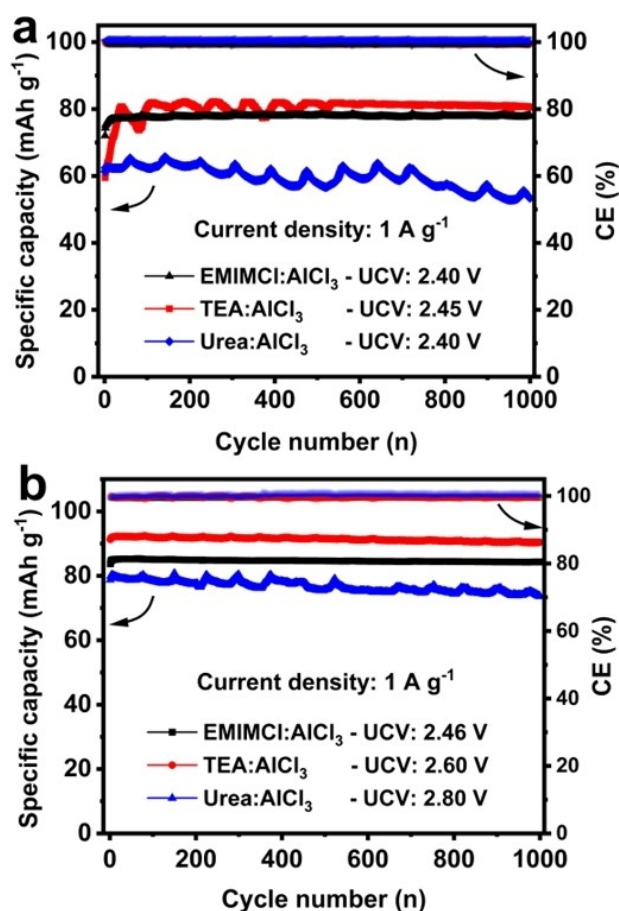

Figure 9. Comparison of specific capacities between AGBs with EMIMCl:AlCl$_3$, TEA:AlCl$_3$ and Urea:AlCl$_3$ electrolytes during long-term cycling at 1 A g^{-1} for 1000 cycles a) before and b) after UCV adjustment.

EMIMCl:AlCl$_3$ exhibited the highest capacity (78 mAh g^{-1}) during the first 50 cycles, maintaining this value consistently throughout the entire 1000 cycles. In contrast, the cell with TEA:AlCl$_3$ experienced a notable increase in capacity from 59 mAh g^{-1} to 81 mAh g^{-1} within the initial 60 cycles, stabilizing at 81 mAh g^{-1} after 500 cycles. This change in capacity is attributed to a reduction in the aluminium anode overpotential (Figure S4), likely resulting from improvements in the aluminium-electrolyte interface. Conversely, the cell with Urea:AlCl$_3$ displayed a comparatively lower capacity of 62 mAh g^{-1}, with a 15% reduction to 52.7 mAh g^{-1} after 1000 cycles, while cells with EMIMCl:AlCl$_3$ and TEA:AlCl$_3$ showed negligible fade. Throughout the long-term cycling, the CE remained consistently above 99% for all the cells.

Additionally, periodic fluctuations in capacity, which occurred approximately every 24 hours were attributed to day-night temperature variations in the lab. These fluctuation was estimated to 1.5, 6, and 15% for EMIMCl:AlCl$_3$, TEA:AlCl$_3$, and Urea:AlCl$_3$, respectively due to the differences in the viscosity and transport properties of the electrolytes.[55] Adjusting UCV resulted in a substantial capacity increase to 85, 92, and 79 mAh g^{-1} corresponding to a capacity enhancements of 10, 13, and 27% with EMIMCl:AlCl$_3$, TEA:AlCl$_3$, and Urea:AlCl$_3$, respectively (Figure 9b and Figure S3). Furthermore, the influence of temperature on capacity fluctuation was minimized to less than 2% in EMIMCl:AlCl$_3$ and TEA:AlCl$_3$, and less than 5% in Urea:AlCl$_3$ after UCV adjustment. The morphological changes in NG cathode after long-term cycling with EMIMCl:AlCl$_3$, TEA:AlCl$_3$ and Urea:AlCl$_3$ electrolytes and the impact of UCV adjustments were characterised by Raman spectra and XRD are shown in Figure 10a and Figure 10b, respectively. Before UCV adjustment, an increase in I$_d$/I$_g$ ratio was observed from 0.105 (pristine NG) to 0.20, 0.45, and 0.13 cycled in EMIMCl:AlCl$_3$ (2.40 V), TEA:AlCl$_3$ (2.45 V) and Urea:AlCl$_3$ (2.40 V), respectively. However, a shift in peak corresponding to G band from 1575 cm^{-1} to 1583 cm^{-1} along with the the shift of peak at 1614 to 1625 cm^{-1} associated to D′ band, is an indication for enhanced lattice disorder and greater AlCl$_4^-$ intercalation-induced defects.[22]

The XRD diffractogram (Figure 9b) show a similar change, revealing a peak shift of 2θ from 26.50° to 26.65° (only after cycling in ILs), corresponding to a decrease in interlayer spacing from 3.4 Å to 3.3 Å, and indicating compressive stress on the graphene layers. Moreover, the increased peak broadening and FWHM values suggest a rise in structural disorder and lattice distortions within the graphite matrix[21,56] The crystallite domain dimensions along the *c-axis* (L$_c$) of NG calculated using the Scherrer equation decreased from 52.13 nm (pristine NG) to 41.71 nm particularly after cycling in ILs EMIMCl:AlCl$_3$ and TEA:AlCl$_3$ (Figure S5). The observed decrease in L$_c$ value can be attributed to the intercalation of larger EMIM$^+$ (109.3 Å) and Et$_3$NH$^+$ (128.7 Å) cations in NG leading to a lower L$_c$ value.[37] Zhang et al showed that the graphite with higher L$_c$ requires more activation energy to enlarge the interlayer spacing between adjacent layers resulting in slower ion kinetics, compared to graphene materials with lower L$_c$ values.[51] Therefore the reduced L$_c$ value of NG cycled in ILs aligns with the
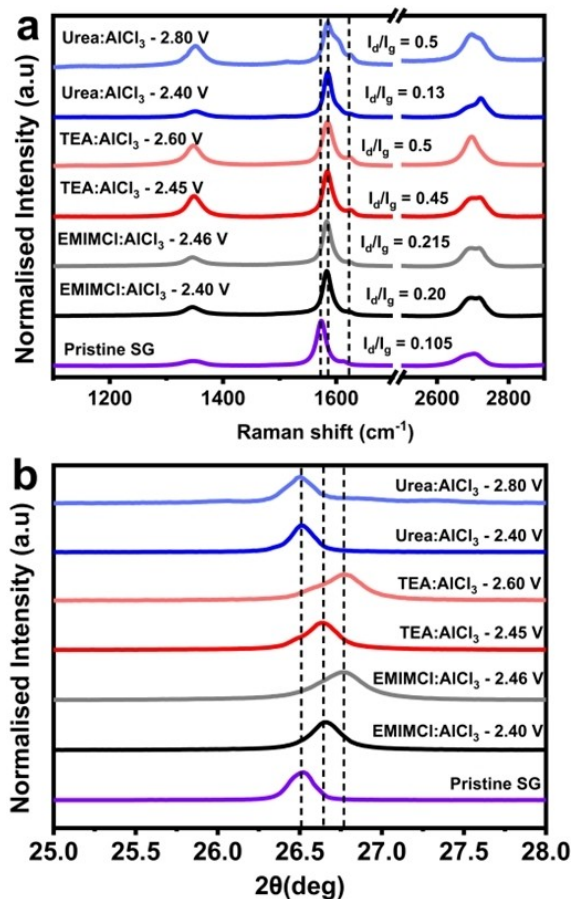
Batteries & Supercaps

Research Article
doi.org/10.1002/batt.202400718

Chemistry Europe
European Chemical
Societies Publishing

Figure 10. Comparison of a) Raman spectra and b) XRD diffractogram of NG cathode between AGBs with EMIMCl:AlCl$_3$, TEA:AlCl$_3$ and Urea:AlCl$_3$ electrolytes after long-term cycling at 1 A g^{-1} for 1000 cycles.

higher capacity observed, as this decrease in L$_c$ value results in faster AlCl$_4^-$ intercalation/deintercalation kinetics.[51,57] In contrast, long-term cycling of NG with Urea:AlCl$_3$ resulted in minimal structural changes as evidence by a marginal increased in the I$_d$/I$_g$ to 0.13 while no significant shift in the 2θ peak and L$_c$ value. This suggest that AlCl$_2$·(urea)$_2^+$ cations do not significantly influence the graphite intercalation reaction.[22] After UCV adjustments, the I$_d$/I$_g$ ratio of NG increased to 0.215, 0.5, and 0.5 cycled in EMIMCl:AlCl$_3$ (2.46 V), TEA:AlCl$_3$ (2.60 V) and Urea:AlCl$_3$ (2.80 V), respectively, showing increased compressive strain as evidenced by a peak shift from 26.50° to 26.75° and a decrease in L$_c$ values to 29.8 nm for NG cycled with EMIMCl:AlCl$_3$ and TEA:AlCl$_3$. The L$_c$ value of NG cycled with Urea:AlCl$_3$ decreased to 34.75 nm, consistent with 27% increase in capacity, yet without a corresponding 2θ peak shift, highlighting the negligible influence of AlCl$_2$·(urea)$_2^+$ cations. These results show the distinct effects of electrolyte type (ILs and DES) and the effect of charging protocol (before and after UCV adjustment) on the NG morphology and AGB capacity after long-term cycling.

3. Conclusions

This study reports on the influence of current density on the electrode potential during the Al dissolution/deposition process and the charge-discharge behaviour of AGB in different 1:1.5 AlCl$_3$-based electrolytes. In the Al–Al symmetric cell, increasing current density above 1 mA cm^{-2} resulted in a notable increase in overpotential up to 200 mV at 5 mA cm^{-2} during the aluminium deposition process in both 1:1.5 TEA:AlCl$_3$ and Urea:AlCl$_3$. Similarly, higher overpotentials during Al deposition process were observed in AGB full-cell during charging step, resulting in incomplete AlCl$_4^-$ intercalation in NG and subsequent capacity fade at higher current densities.

Adjusting the UCV in the AGB full-cell for each current density improved specific capacities up to 1 A g^{-1} and led to remarkable reduction in capacity fading less than 7% across all electrolytes. This shows a significant improvement compared to the fading rates of 14, 33, and 53% in EMIMC:AlCl$_3$, TEA:AlCl$_3$ and Urea:AlCl$_3$, respectively, before UCV adjustment. The AGB cells exhibited substantial improvements in energy density, with a 48% increase observed with TEA:AlCl$_3$ and an impressive 250% increase with Urea:AlCl$_3$ at 1 A g^{-1} after UCV adjustment. Structural analyses through Raman spectroscopy and XRD provided insights into the changes within the graphite structure. These changes were attributed to the compressive stresses caused by cations (EMIM$^+$ and Et$_3$NH$^+$) in addition to the structural deformations induced by electrolyte interactions and AlCl$_4^-$ intercalation at different UCVs. Systematic monitoring of anode overpotential during charging and discharging steps may provide valuable insights for optimizing anode morphology, such as increasing its active surface area for improved performance at high current densities.

Author Contributions

C.M. designed the work, conceptualized, and conducted the experiments, analysed the data, and wrote the manuscript. J.F.D supervised the project and reviewed the manuscript. All authors have approved the final version of the manuscript.

Conflict of Interests

The authors declare no conflict of interest.

Batteries & Supercaps

Research Article
doi.org/10.1002/batt.202400718

Chemistry Europe
European Chemical
Societies Publishing

Data Availability Statement

The data that support the findings of this study are available in the supplementary material of this article.

[1] D. Larcher, J. M. Tarascon, *Nat. Chem.* **2015**, *7*, 19–29.
[2] P. K. Nayak, L. Yang, W. Brehm, P. Adelhelm, *Angew. Chem. Int. Ed.* **2018**, *57*, 102–120.
[3] B. Dunn, H. Kamath, J. M. Tarascon, *Science* **2011**, *334*, 928–935.
[4] T. M. Gür, *Energy Environ. Sci.* **2018**, *11*, 2696–2767.
[5] G. A. Elia, K. Marquardt, K. Hoeppner, S. Fantini, R. Lin, E. Knipping, W. Peters, J.-F. Drillet, S. Passerini, R. Hahn, *Adv. Mater.* **2016**, *28*, 7564–7579.
[6] T. B. Reddy, *Linden's Handbook of Batteries*, 4th ed., McGraw-Hill, New York, **2011**, p. 1.10.
[7] F. Ambroz, T. J. Macdonald, T. Nann, *Adv. Energy Mater.* **2017**, *7*, 1602093.
[8] K. V. Kravchyk, M. V. Kovalenko, *Adv. Energy Mater.* **2020**, *10*, 202002151.
[9] Y. Long, H. Li, M. Ye, Z. Chen, Z. Wang, Y. Tao, Z. Weng, S.-Z. Qiao, Q.-H. Yang, *Energy Storage Mater.* **2021**, *34*, 194–202.
[10] L. C. Loaiza, N. Lindahl, P. Johansson, *J. Electrochem. Soc.* **2023**, *170*, 030512.
[11] R. Böttcher, A. Ispas, A. Bund, *Electrochem. Commun.* **2020**, *115*, 106720.
[12] N. Lindahl, P. Johansson, *Energy Adv.* **2023**, *2*, 420–429.
[13] E. Faegh, B. Ng, D. Hayman, W. E. Mustain, *Nat. Energy* **2021**, *6*, 21–29.
[14] S. He, J. Wang, X. Zhang, W. Chu, S. Zhao, D. He, M. Zhu, H. Yu, *J. Mater. Chem. A.* **2023**, *11*, 17020–17026.
[15] S. Wang, Y. Guo, X. Du, L. Xiong, Z. Huang, X. Li, M. Ma, Z. Liang, Y. Xie, *Energy Storage Mater.* **2023**, *60*, 102826.
[16] J. Zheng, D. C. Bock, T. Tang, Q. Zhao, J. Yin, K. R. Tallman, G. Wheeler, X. Liu, Y. Deng, S. Jin, A. C. Marschilok, E. S. Takeuchi, K. J. Takeuchi, L. A. Archer, *Nat. Energy* **2021**, *6*, 398–406.
[17] C. Mukundan, M. Lie, J.-F. Drillet, *Sustain. Energy & Fuels* **2025**, Advance Article.
[18] K. V. Kravchyk, M. V. Kovalenko, *Commun. Chem.* **2020**, *3*, 120.
[19] C. Mukundan, M. Eckert, J.-F. Drillet, *Batteries & Supercaps* **2023**, *6*, e202300042.
[20] H. Xu, T. Bai, H. Chen, F. Guo, J. Xi, T. Huang, S. Cai, X. Chu, J. Ling, W. Gao, Z. Xu, C. Gao, *Energy Storage Mater.* **2019**, *17*, 38–45.
[21] K. L. Ng, T. Dong, J. Anawati, G. Azimi, *Adv. Sustainable Syst.* **2020**, *4*, 2000074.
[22] K. L. Ng, M. Malik, E. Buch, T. Glossmann, A. Hintennach, G. Azimi, *Electrochim. Acta* **2019**, *327*, 135031.
[23] M. Angell, C.-J. Pan, Y. Rong, H. Dai, *Proc. Natl. Acad. Sci. USA* **2017**, *114*, 834–839.
[24] C. Xu, W. Zhang, P. Li, S. Zhao, Y. Du, H. Jin, Y. Zhang, Z. Wang, J. Zhang, *Sustain. Energy Fuels* **2020**, *4*, 121–127.
[25] F. Jach, M. Wassner, M. Bamberg, E. Brendler, G. Frisch, U. Wunderwald, J. Friedrich, *ChemElectroChem* **2021**, *8*, 1988–1992.
[26] N. Canever, N. Bertrand, T. Nann, *Chem. Commun.* **2018**, *54*, 11725–11728.
[27] M. C. Lin, M. Gong, B. Lu, Y. Wu, D.-Y. Wang, M. Guan, M. Angell, C. Chen, J. Yang, B.-J. Hwang, H. Dai, *Nature* **2015**, *520*, 325–328.
[28] W. Zhou, P. H. L. Sit, *ACS Omega* **2020**, *5*, 18289–18300.
[29] K. Ji, J, Han, A. Hirata, T. Fujita, Y. Shen, S. Ning, P. Liu, H. Kashani, Y. Tian, Y. Ito, J.-I. Fujita, Y. Oyama, *Nat. Commun.* **2019**, *10*, 275.
[30] C.-J. Pan, C. Yuan, G. Zhu, H. Dai, *Proc. Natl. Acad. Sci. USA* **2018**, *115*, 5670–5675.
[31] M. L. Agiorgousis, Y. Y. Sun, S. Zhang, *ACS Energy Lett.* **2017**, *2*, 689–693.
[32] P. Bhauriyal, A. Mahata, B. Pathak, *Phys. Chem. Chem. Phys.* **2017**, *19*, 7980–7989.
[33] K. V. Kravchyk, M. V. Kovalenko, *Adv. Energy Mater.* **2019**, *9*, 1901749.
[34] S. Wang, K. V. Kravchyk, F. Krumeich, M. V. Kovalenko, *ACS Appl. Mater. Interfaces* **2017**, *9*, 28478–28485.
[35] S. C. Jung, Y. J. Kang, D.-J. Yoo, J. W. Choi, Y.-K. Han, *J. Phys. Chem. C* **2016**, *120*, 13384–13389.
[36] J. Qiao, H. Zhao, Z. Liu, H. Wen, J. Du, G. Wei, C. He, J. Yang, *Ionics* **2020**, *26*, 245–254.
[37] H. Xu, H. Chen, H. Lai, Z. Li, X. Dong, S. Cai, X. Chu, C. Gao, *J. Energy Chem.* **2020**, *45*, 40–44.
[38] H. Chen, H. Xu, T. Huang, C. Gao, *Sci. Adv.* **2017**, *3*, eaao7233.
[39] X. Dong, H. Chen, H. Lai, L. Wang, J. Wang, W. Fang, C. Gao, *J. Energy Chem.* **2022**, *66*, 38–44.
[40] Z. Li, J. Li, X. Li, W. Zhang, *J. Power Sources* **2019**, *467*, 134–140.
[41] X. Dong, H. Xu, H. Chen, L. Wang, J. Wang, W. Fang, C. Chen, M. Salman, Z. Xu, C. Gao, *Carbon* **2019**, *148*, 134–140.
[42] D. Zhang, W. Zhang, S. Zhang, X. Ji, L. Li, *J. Energy Storage* **2023**, *60*, 106678.
[43] Q. Zhao, J. Zheng, L. Deng, L. Archer, *J. Mater. Chem. A* **2020**, *8*, 23231–23238.
[44] N. Li, D. She, K. Zhang, H.-S. Chen, W.-L. Song, S. Jiao, *ChemSusChem* **2022**, *15*, e202201390.
[45] S. Choi, H. Go, G. Lee, Y. Tak, *Phys. Chem. Chem. Phys.* **2017**, *19*, 8653–8656.
[46] H. Go, M. R. Raj, Y. Tak, G. Lee, *Electroanalysis* **2022**, *34*, 1308–1317.
[47] D. Muñoz-Torrero, P. Leung, E. García-Quismondo, E. Ventosa, M. Anderson, J. Palma, R. Marcilla, *J. Power Sources* **2018**, *374*, 77–83.
[48] K. L. Ng, Z. Lu, Y. Wang, C. V. Singh, G. Azimi, *Phys. Chem. Chem. Phys.* **2021**, *125*, 15145–15154.
[49] V. Elterman, P. Y. Shevelin, L. A. Yolshina, E. G. Vovkotrub, A. V. Borozdin, *J. Mol. Liq.* **2020**, *320*, 114482.
[50] G. A. Elia, K. Hoeppner, R. Hahn, *Batteries & Supercaps* **2021**, *4*, 368–373.
[51] L. Zhang, L. Chen, H. Luo, X. Zhou, Z. Liu, *Adv. Energy Mater.* **2017**, *7*, 1700034.
[52] M. Angell, G. Zhu, M. C. Lin, Y. Rong, H. Dai, *Adv. Funct. Mater.* **2020**, *30*, 1901928.
[53] J. H. Xu, D. E. Turney, A. L. Jadhav, R. J. Messinger, *ACS Appl. Energ. Mater.* **2019**, *2*, 7799–7810.
[54] T.-S. Lee, S. B. Patil, Y.-T. Kao, J.-Y. An, Y.-C. Lee, Y.-H. Lai, C.-K. Chang, Y.-S. Cheng, Y.-C. Chuang, H.-S. Sheu, C.-H. Wu, C.-C. Yang, R.-H. Cheng, C.-Y. Lee, P.-Y. Peng, L.-H. Lai, H.-H. Lee, D.-Y. Wang, *ACS Appl. Mater. Interfaces* **2020**, *12*, 2572–2580.
[55] T. Schoetz, J. H. Xu, R. J. Messinger, *ACS Appl. Energ. Mater.* **2022**, *6*, 2845–2854.
[56] Z. Xing, Y. Qi, Z. Jian, X. Ji, *ACS Appl. Mater. Interfaces* **2017**, *9*, 4343–4351.
[57] J. H. Xu, T. Schoetz, J. R. McManus, V. R. Subramanian, P. W. Fields, R. J. Messinger, *J. Electrochem. Soc.* **2021**, *168*, 060514.